

Chemical, physical, structural and morphological characterization of the electric arc furnace dust

Janaína G.M.S. Machado^{a,*}, Feliciane Andrade Brehm^b,
Carlos Alberto Mendes Moraes^b, Carlos Alberto dos Santos^c,
Antônio Cezar Faria Vilela^a, João Batista Marimon da Cunha^d

^a Laboratório de Siderurgia/LASID, Universidade Federal do Rio Grande do Sul, UFRGS/PPGEM Centro de Tecnologia,
AV. Bento Gonçalves 9500 CEP, 91501-970 Caixa postal 15021, Porto Alegre, RS, Brazil

^b Núcleo de Caracterização de Materiais/NucMat, Universidade do Vale do Rio dos Sinos, UNISINOS, São Leopoldo, RS, Brazil

^c Núcleo de Educação a Distância, Universidade Estadual do Rio Grande do Sul, UERGS, Porto Alegre, RS, Brazil

^d Instituto de Física, Universidade Federal do Rio Grande do Sul, UFRGS, Campus do Vale, Porto Alegre, RS, Brazil

Received 28 September 2005; received in revised form 14 January 2006; accepted 17 January 2006

Available online 21 February 2006

Abstract

Electric arc furnace dust (EAFD) is a hazardous industrial waste generated in the collection of particulate material during steelmaking process via electric arc furnace. Important elements to the industry such as, Fe and Zn are the main ones in EAFD. Due to their presence, it becomes very important to know how these elements are combined before studying new technologies for its processing. The aim of this work was to carry out a chemical, physical, structural and morphological characterization of the EAFD. The investigation was carried out by using granulometry analysis, chemical analysis, scanning electron microscopy (SEM), energy dispersive spectroscopy via SEM (EDS), X-ray mapping analysis via SEM, X-ray diffraction (XRD) and Mössbauer spectroscopy. By XRD the following phases were detected: ZnFe_2O_4 , Fe_3O_4 , MgFe_2O_4 , FeCr_2O_4 , $\text{Ca}_{0.15}\text{Fe}_{2.85}\text{O}_4$, MgO , Mn_3O_4 , SiO_2 and ZnO . On the other hand, the phases detected by Mössbauer spectroscopy were: ZnFe_2O_4 , Fe_3O_4 , $\text{Ca}_{0.15}\text{Fe}_{2.85}\text{O}_4$ and FeCr_2O_4 . Magnesium ferrite (MgFe_2O_4), observed in the XRD pattern as overlapped peaks, was not identified in the Mössbauer spectroscopy analysis.

© 2006 Elsevier B.V. All rights reserved.

Keywords: EAFD; Characterization; XRD; Mössbauer spectroscopy; SEM

1. Introduction

Electric arc furnace dust (EAFD) is a solid waste generated during the steelmaking process. It is classified according to NBR 10005 [1] as dangerous solid waste-class I, because the elements Pb e Cd leach in water exceeding the maximum limits permitted by the NBR 10004 [2,3]. The State Foundation for Environmental Protection of Rio Grande do Sul – FEPAM – requires that this waste must be stored in an appropriate place protected from rain. Due to the great amount generated, 12–14 kg of dust per ton of steel, an evaluation of the steel recycling alternatives is necessary.

The world generation of EAFD is estimated to be around 3.7 million tonnes per year. Plants from Europe generate around 500,000 and 900,000 tonnes of dusts per year. The great generators are Italy (170.000 tonnes per year), Germany (160.000 tonnes per year), France (140.000 tonnes per year) and Spain (115.000 tonnes per year). About 700.000–800.000 tonnes per year of EAFD are generated in United States of America, which is increasing 4–6% per year [4].

In general, and especially in developed countries, the treatment processes of the EAFD commonly used aim mainly the recovering of zinc. This is due to the fact that in the last 40 years this element has been used progressively in the galvanizing process of the carbon steel, which has increased its price in those countries.

When galvanized scrap is used in the EAF, most of the zinc from the steel scrap ends up in the dust and fume due to its

* Corresponding author. Tel.: +51 33167074; fax: +51 33167116.
E-mail address: jana@ct.ufrgs.br (J.G.M.S. Machado).

very low solubility in molten steel and slag, and, especially, because zinc vapor pressure is higher than iron vapor pressure at steelmaking temperature. Vapor zinc is carried out the furnace with other gaseous or particulate compounds generated during steelmaking reactions, generating compounds like ZnO and ZnFe₂O₄. According to Leclerc [5], when some zinc particles are in contact with iron particles at high temperatures in an oxidizing atmosphere, zinc ferrite formation will occur in the furnace and in the evacuation system. The problem is that zinc does not come out alone, other elements evaporate and are collected in the dedusting system originating the EAFD.

In Brazil, the galvanizing steel recycling is not so intensive, so the scrap used in the steelmaking has low zinc content, which disables the use of the commercialized technologies all over the world. The low amounts of zinc lead to the necessity of recirculation or recycling the dust in the EAF before the use of available technologies for the Zn reclamation in an economical viability [6].

As chemical and structural characterization of solid waste is a very important stage to evaluate the recycling feasibility, several analytical techniques have been used to study EAFD. Comparing the chemical analysis results with X-ray diffraction (XRD), Mössbauer spectroscopy and scanning electron microscopy (SEM) becomes possible to determine and to quantify the phases present in the EAFD. So, the aims of this work are the chemical, physical, structural and morphological characterization of the EAFD. Moreover, the use of several characterization techniques is important because the findings about the existence of two Zn oxides are of great importance to its recycling as raw material:

- (1) to obtain metallic zinc to zinc industry,
- (2) to obtain metallic iron to iron and steelmaking industry, and even
- (3) for its recycling in the civil construction, because depending on the presence and amount of zinc oxide the retardation in the hydration reactions may occur, which can result in a barrier for its use in this application.

2. Experimental

The EAFD was sampled from the dust collecting system of a steelmaking plant in Southern Brazil. This company is characterized by producing steels with a varied chemical composition.

2.1. Granulometry analysis

The EAFD granulometric distribution and the medium diameter of its particles were evaluated. A Laser Granulometer – model 1064 – from Cilas was used.

2.2. Chemical characterization

The chemical characterization of EAFD focused in the determination of specific elements such as iron, zinc, calcium, chromium and magnesium. The analysis was carried out via

inductively coupled plasma atomic emission spectroscopy (ICP-AES).

The digestion is the first step in the preparation of the sample to determine its chemical composition, where the solid sample becomes a liquid solution.

Brehm et al. [7] suggested that to obtain a complete digestion of the EAFD, the methodology must be divided into two stages:

- 1st stage: digestion via electric plate;
- 2nd stage: alkaline fusion of the insoluble waste from the 1st stage.

To accelerate this procedure, the digestion via microwave oven was used, instead of electric plate (performance time \approx 3 h). The stage performance time was about 45 min using microwave, and the obtained solution was the same. A flow diagram of the used methodology is shown in Fig. 1.

2.3. X-ray diffraction

The structural characterization of EAFD was performed through X-ray diffraction analysis in a Siemens appliance model D500. X-ray patterns of samples powdered to 400 mesh were obtained with monochromated Cu K α radiation in the 2θ -range from 2° to 140° with a scan step of $0.05^\circ 2\theta$, and fixed counting time of 1s for each step. The pattern was analyzed by using the Philips X-Pert Software.

2.4. Mössbauer spectroscopy

Absorbers for Mössbauer spectroscopy measurements were prepared with appropriate amounts of ground (400 mesh) material to satisfy the ideal absorber thickness approximation [8]. The spectrum was taken at room temperature using a constant acceleration electromechanical drive system with a multichannel analyzer for collecting and storing the data. The velocity scale was calibrated using a high-purity 6 μ m thick Fe foil. The hyperfine parameters were obtained by a least-squares procedure assuming Lorentzian line shapes constrained to equal halfwidths. ⁵⁷Co in rhodium was used at room temperature as a

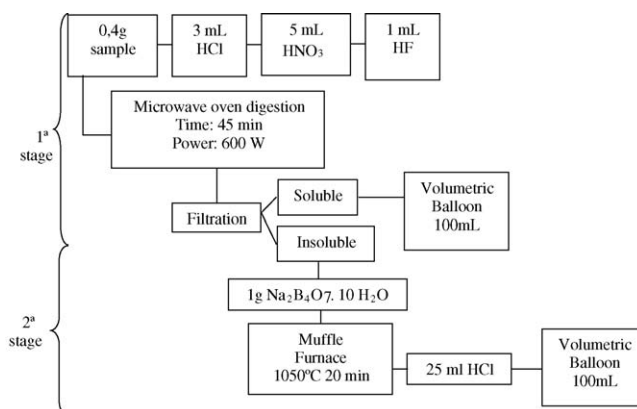


Fig. 1. Methodology used for the EAFD sample digestion.

source, with nominal activity of 10 mCi. Typical errors are $\pm 3\%$ on hyperfine parameters and $\pm 5\%$ on site occupancies. All the data treatment process was performed with a Windows version of the Btall Program.

2.5. Scanning electron microscopy and micro-analysis

Scanning electron microscopy (SEM) with X-ray energy dispersive spectrometry (EDS) was performed to gain further knowledge of the EAFD particles structure, morphology and their chemical composition. The samples were pressed in an organic resin by cold cure, grounded with silicon carbide paper and polished with diamond suspension. The samples were carbon coated for imaging and EDX analysis. The same samples were also subjected to the element distribution analysis (O, Fe, Zn, Mg, Ca, Cr, Si, Mn) through X-ray mapping analysis via SEM.

3. Results and discussion

3.1. Granulometric analysis

The granulometric distribution analysis of the EAFD is shown in Fig. 2.

The mean particle diameter of EAFD determined by laser granulometer was $1.88 \mu\text{m}$. It can be seen from Fig. 2 that the EAFD has a heterogeneous distribution of particle size, where 60% have size between 0.90 and $4.30 \mu\text{m}$. Such an irregular granulometric distribution is in agreement with that published by Mantovani et al. [9]. Probably, this is due to the agglomerated state of the particles because this material is well known to have fine granulometry.

Xia and Pickles [10] also pointed out that the particles in EAFD tend to exist as aggregates consisting of very fine individual particles. Most of the individual particles were lower than $1 \mu\text{m}$. Takano et al. [6] determined in two different types of EAFD that almost 90% of the particles are lower than $10 \mu\text{m}$.

Menad et al. [11] analyzed the particle size distribution of EAFD with two screen sizes (i.e., 500 and $15 \mu\text{m}$). They observed that the dust is very fine; more than 70% of particles are lower than $15 \mu\text{m}$. They also observed that the metals are more concentrated in the fine fraction of the waste.

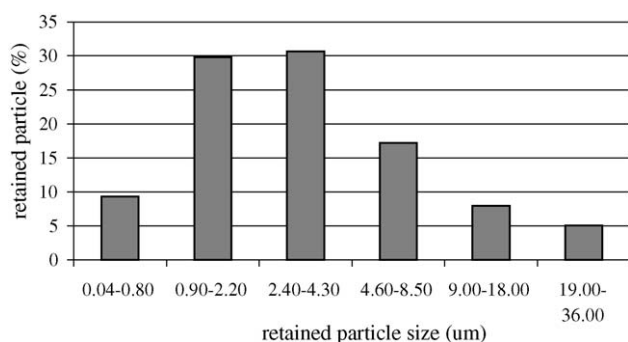


Fig. 2. Granulometric distribution of EAFD.

Table 1
Chemical composition of EAFD

Element	%
Fe	48.96
Zn	9.24
Ca	3.28
Cr	2.90
Mg	1.65

3.2. Chemical characterization

The result of the chemical analysis of EAFD is presented in Table 1.

The chemical analysis result from Table 1 is expressed in elemental form. Usually, this kind of analysis is expressed in the most stable oxides forms [12–15]. However, the use of other techniques to characterize EAFD such as, X-ray diffraction analysis, Mössbauer spectroscopy and scanning electron microscopy with EDS, has shown that in fact the elements are not present as the most stables oxide forms as pointed out in those works.

According to Nyirenda [16], for the EAFD from carbon steel, zinc contents usually are between 11.12 and 26.9 wt.%. The zinc contents in the EAFD are between 1.77 and 6.22% from stainless steel. Fe and Zn contents found in the EAFD from the present work (Table 1) can be considered as intermediate values compared to those found in the literature, which is also coherent with the types of steel (carbon, stainless, and tool) produced in the steelmaking plant that generates this EAFD.

3.3. X-ray diffraction

Fig. 3 shows the X-ray diffraction pattern of the EAFD sample.

As it can be seen, ZnFe_2O_4 , Fe_3O_4 , MgFe_2O_4 , FeCr_2O_4 , Mn_3O_4 , MgO , SiO_2 , $\text{Ca}_{0.15}\text{Fe}_{2.85}\text{O}_4$ and ZnO are present in the EAFD sample. However, except for SiO_2 and ZnO , the signals from all phases exhibit overlapping in some extent, as shown in Fig. 3. Because of such overlapping, also observed by Heck [17] the presence of these phases cannot be unequivocally assured. As it will be shown, to improve the phase identification in EAFD samples it is necessary to use other techniques like, for example, Mössbauer spectroscopy and scanning electron microscopy with energy dispersive spectroscopy and X-ray mapping analysis. The Mössbauer spectroscopy was used for investigation of the ferrous oxide phases ZnFe_2O_4 , Fe_3O_4 , MgFe_2O_4 , FeCr_2O_4 and $\text{Ca}_{0.15}\text{Fe}_{2.85}\text{O}_4$.

3.4. Mössbauer spectroscopy

The Mössbauer spectrum for EAFD is displayed in Fig. 4. The isomer shift (IS), quadrupole splitting (QS), hyperfine field (H_{eff}) and line width (Γ) obtained from best fitted Mossbauer spectrum line are presented in Table 2.

It is interesting to observe that the magnesium-ferrite phase (MgFe_2O_4) identified through XRD in overlapped peaks was not observed in the Mössbauer spectra. Comparing Mössbauer

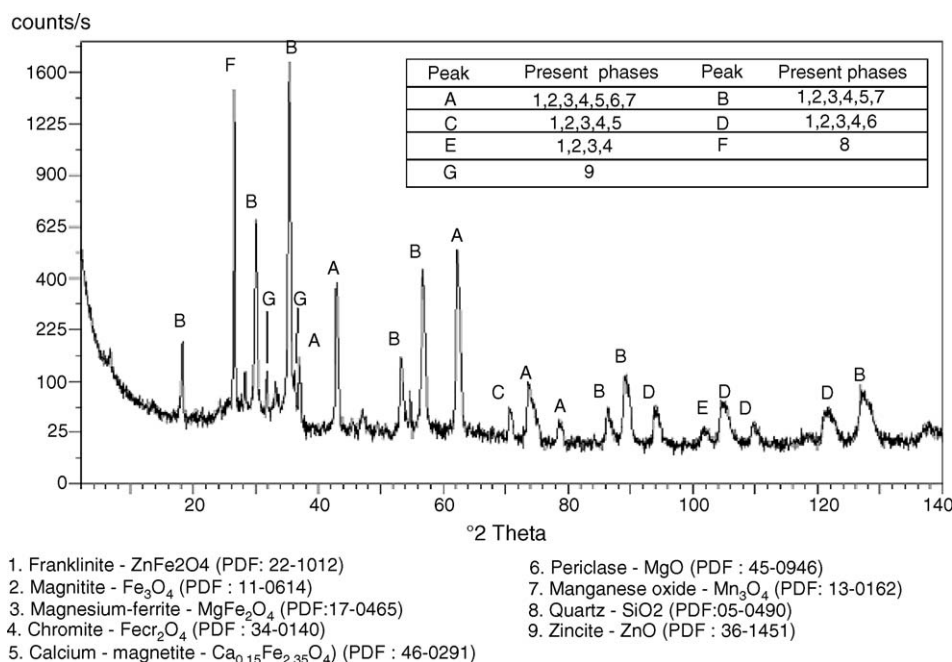


Fig. 3. X-ray diffraction (XRD) pattern of EAFD.

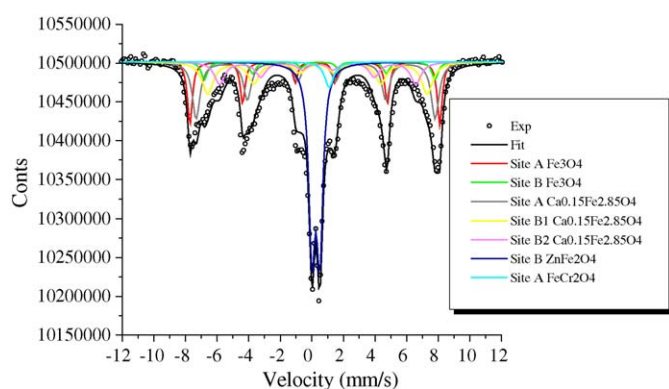


Fig. 4. Mössbauer spectrum of EAFD.

results with the Mg amount determined via ICP, it may be suggested that such phase is not present in the dust.

The Mössbauer parameters obtained for Fe₃O₄, ZnFe₂O₄ and FeCr₂O₄ in the EAFD are in agreement with those reported in the literature [18–20]. Values around 0.50 mm/s for the line width are commonly found in the literature. Spectrum with wide lines may indicate, among other things, sample disordering [20].

Table 2
Mössbauer Parameters used in the spectrum fit of the EAFD at room temperature

Sample	Phase	H _{eff} (kOe)	IS (mm/s)	QS (mm/s)	Γ (mm/s)	
EAFD	Fe ₃ O ₄	Site A	491	0.30	−0.01	0.37
		Site B	453	0.60	0.01	0.47
	ZnFe ₂ O ₄	Site A	–	0.35	0.50	0.47
	FeCr ₂ O ₄	Site B	–	–	1.1	0.70
Ca _{0.15} Fe _{2.85} O ₄	Site A	Site A	470	0.38	−0.06	0.59
		Site B	408	0.47	0.01	0.83

The hyperfine field for the site assigned as B in Ca_{0.15}Fe_{2.85}O₄ is an average between two fitted values, as illustrated in Fig. 4. Such a behavior is due to the fact that calcium substitutes iron randomly at the site B, occupying in a disordered way the iron place in the magnetite B site. The result is that, for each unit-cell, there are different hyperfine interactions and, consequently, a hyperfine magnetic field distribution in this site [21].

Barcellos pointed out that one of the main oxides characteristics is the partial substitution of the iron for other cations [22]. The magnetic properties of the spinels are very sensitive to the nature of the metallic cations present in the compound and to their distribution between the A and B sites. In the magnetite, some cations have been noted replacing the iron: Al³⁺, Mn²⁺, Ni²⁺, Cu²⁺, Co²⁺, Zn²⁺, Ca²⁺ e Ge²⁺. The magnetic properties of the iron oxides are very affected by this replacement. In general, the reduction of the magnetic ordering temperature and consequently the reduction of hyperfine magnetic field are observed. The hyperfine field reduction occurs because the cation presence makes the interaction among iron ions weaker. In this case it can be considered that each impurity present in the structure removes one element from the Fe³⁺–Fe³⁺ coupling.

Table 3 shows the ferrous quantification in the oxide phases found in the EAFD according to Mössbauer spectroscopy.

One of the most important characteristics of the Mössbauer spectroscopy technique is its selectivity. If the emitter Mössbauer isotope is, for example, ⁵⁷Fe, the resonant absorption may only occur if there are identical nucleus inside the absorbent. In this way, even if the sample shows a great variety of compounds, only the ones, which have a Mössbauer nucleus in their constitution, will be detected. Considering that the EAFD does not present only iron in its constitution, the results of the Mössbauer spectroscopy and the ICP analysis (Fe and Zn con-

Table 3
Quantification of ferrous in the oxide phases present in the EAFD according to the Mössbauer spectroscopy

Phase		EAFD (%)
Fe ₃ O ₄	Site A	14.82
	Site B	5.33
ZnFe ₂ O ₄	Site A	27.05
FeCr ₂ O ₄	Site B	2.80
Ca _{0.15} Fe _{2.85} O ₄	Site A	21.35
	Site B1	17.39
	Site B2	11.27

tent) were used to determine the amount of the main oxides phases (Fe₃O₄, ZnFe₂O₄, FeCr₂O₄, Ca_{0.15}Fe_{2.85}O₄ e ZnO). Analyzing the results of both characterization techniques it was possible to provide a quantitative estimation of the ZnFe₂O₄ phase, and indirectly a quantitative estimation of the ZnO phase. The amount of ZnO was determined as follows:

- 1st step: determination ZnFe₂O₄ amount:

$$\%Fe_{(ZnFe_2O_4)} = \frac{\%Fe_{total(via\ ICP)} \times \%Fe_{(ZnFe_2O_4)(via\ Mössbauer)}}{100}$$

$$\%ZnFe_2O_4 = \frac{\%Fe_{(ZnFe_2O_4)} \times \bar{M}_{Fe(ZnFe_2O_4)}}{\bar{M}_{(ZnFe_2O_4)}}$$

- 2nd step: determination ZnO amount:

$$\%Zn_{(ZnFe_2O_4)} = \frac{\%ZnFe_2O_4 \times \bar{M}_{(Zn)}}{\bar{M}_{(ZnFe_2O_4)}}$$

$$\%Zn_{ZnO} = \%Zn_{total(via\ ICP)} - \%Zn_{(ZnFe_2O_4)}$$

$$\%ZnO = \frac{\%Zn_{(ZnO)} \times \bar{M}_{(ZnO)}}{\bar{M}_{(Zn)}}$$

Where, %Fe(ZnFe₂O₄): %Fe in ZnFe₂O₄ phase; %Fe_{total(via ICP)}: wt.% of total Fe determined via ICP; %Fe_{(ZnFe₂O₄)(via Mössbauer)}: %Fe in ZnFe₂O₄ phase determined via Mössbauer; % ZnFe₂O₄: %ZnFe₂O₄ in EAFD; $\bar{M}_{Fe(ZnFe_2O_4)}$: molar weight of Fe in ZnFe₂O₄ phase; $\bar{M}_{(ZnFe_2O_4)}$: molar weight of ZnFe₂O₄ phase; %Zn(ZnFe₂O₄): % Zn in ZnFe₂O₄ phase; $M_{(Zn)}$: molar weight of Zn; %Zn_(ZnO): % Zn in ZnO phase; %Zn_{total(via ICP)}: wt.% of total Zn determined via ICP; $\bar{M}_{(ZnO)}$: molar weight of ZnO.

Based on these calculations, Table 4 shows the analyzed sample composition taking into account the results from these two techniques.

Table 4
Quantification of the mainly oxides phases in the EAFD

Phase	EAFD (%)
Fe ₃ O ₄	14
ZnFe ₂ O ₄	29
FeCr ₂ O ₄	6
Ca _{0.15} Fe _{2.85} O ₄	35
ZnO	2

The total amount of the phases found in the EAFD was not 100% because some elements with minor amounts were not analyzed via chemical technique (ICP), such as silicon, usually found in EAFD. As it can be seen in Table 4, more than 80% of the oxide phases contain iron in their constitution which makes the carbothermic reduction study attractive to recover this element [23].

3.5. Scanning electron microscopy and micro-analysis

Fig. 5 shows a general distribution of EAFD particles, where most particles are spherical.

This shape is in agreement with the main generation mechanism, i.e. ejection of the slag and metal particles by bubble-burst [6]. This morphology has also been observed in previous works [24,25].

Huber et al. [13] observed via SEM that most EAFD particles are submicronic and 80 wt.% are smaller than 20 μm. An agglomerated morphology is predominant with fine particles forming aggregates or covering larger particles.

The morphological aspects of EAFD were also observed via SEM analysis by MENAD et al. [11]. This technique shows that these materials contain very fine particles, i.e., smaller than 10 μm.

Fig. 6 shows a typical morphology of EAFD containing a dendritic structure, and Table 5 shows the result of EDS analysis of areas 1 and 2 identified in Fig. 6.

Based on the result from EDS, it can be seen that the higher contributions are due to Fe, Cr and O in the clearer region and to Fe, Ca, Si and O in the darker one. Cruells et al. [26] also observed via EDS in an EAFD particle a polygonal precipitate containing iron as the main element and also chromium. Mantovani et al. [9] often observed in the EAFD particles with dendritic structure containing a spinel-ferrite crystal (white) enclosed in a calcium–iron–silicate glass (gray). Also according to the authors this structure is related to the rapid cooling of particle.

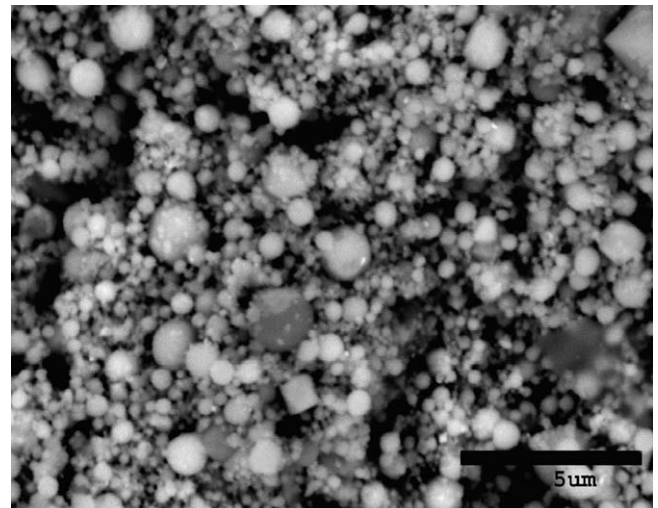


Fig. 5. Scanning electron micrograph (magnification 7500×) of EAFD particles.

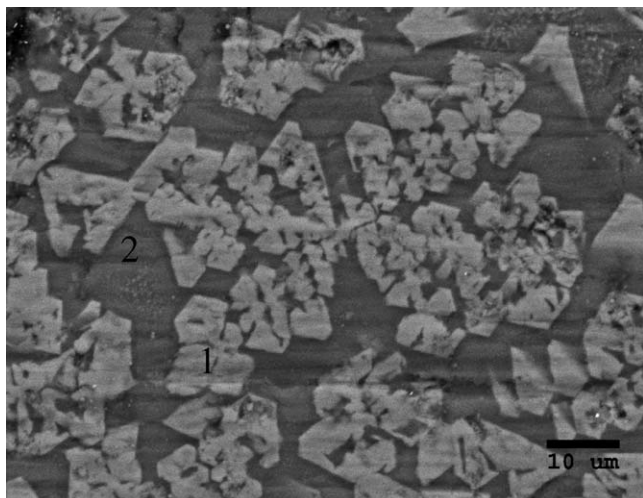


Fig. 6. Scanning electron micrograph (magnification 1500×) showing a dendritic structure of EAFD.

Table 5
Energy dispersive spectrometry (EDS) of area (1) rich in Fe, Cr and O; and area (2) rich in Fe, Ca, Si and O showed in Fig. 6

Element	Area 1 (%)	Area 2 (%)
Fe	39.84	34.95
Cr	33.62	3.38
O	10.12	13.51
Al	2.54	2.56
Si	0.60	10.93
Mg	5.29	0.38
Mn	5.47	1.50
Ca	2.51	32.79

Figs. 7 and 8 show typical scanning electron micrographs of EAFD. Tables 6 and 7 give the results of EDS analysis of areas 1 and 2 identified in Figs. 7 and 8.

It can be said that area 1, in both figures, is probably magnetite (Fe_3O_4). In area 2, in both Figures, it was observed that the

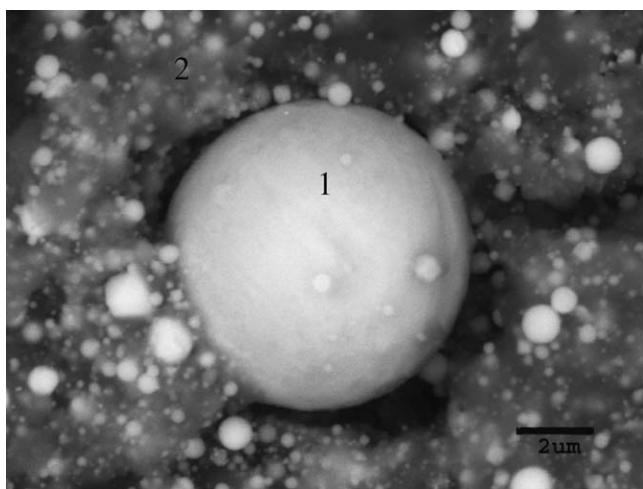


Fig. 7. Scanning electron micrograph (magnification 8000×) showing two regions: (1) rich in Fe and O; (2) rich in Fe and Zn.

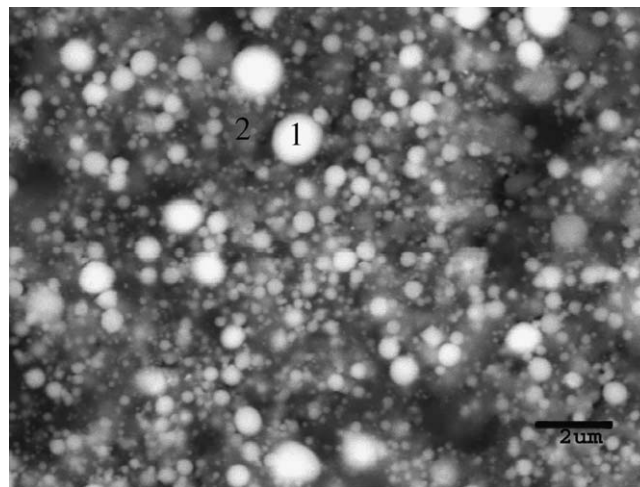


Fig. 8. Scanning electron micrograph (magnification 8000×) showing two regions: (1) rich in Fe and O; (2) rich in Fe and Zn.

Table 6
Energy dispersive spectrometry (EDS) of areas 1 and 2 in Fig. 7

Element	Area 1 (%)	Area 2 (%)
Fe	90.34	59.55
Zn	–	22.63
O	8.41	2.83
Cl	–	2.93
Si	0.25	2.74
Mg	–	1.58
K	–	2.00
Ca	0.39	1.91
Cr	0.62	2.62
S	–	1.21

particles are very fine and iron and zinc are present in a high amount. Probably it is the region where the franklinite phase (ZnFe_2O_4) is present.

Fig. 9 shows a secondary electron image of an EAFD region and the X-ray mapping for the elements Fe, Zn, Ca, Cr, Si, Mg, Mn and O present in the dust.

This figure indicates that oxygen is practically distributed along all the sample, which suggests the presence of metal–oxygen structural forms. There are regions in which the

Table 7
Energy dispersive spectrometry (EDS) of areas 1 and 2 in Fig. 8

Element	Area 1 (%)	Area 2 (%)
Fe	72.55	58.09
Zn	12.64	22.37
O	5.64	2.49
Cl	1.10	3.86
Si	1.79	2.59
Mg	1.46	1.77
K	–	1.63
Ca	1.12	2.09
Cr	–	0.71
Mn	3.60	2.78
S	–	1.62

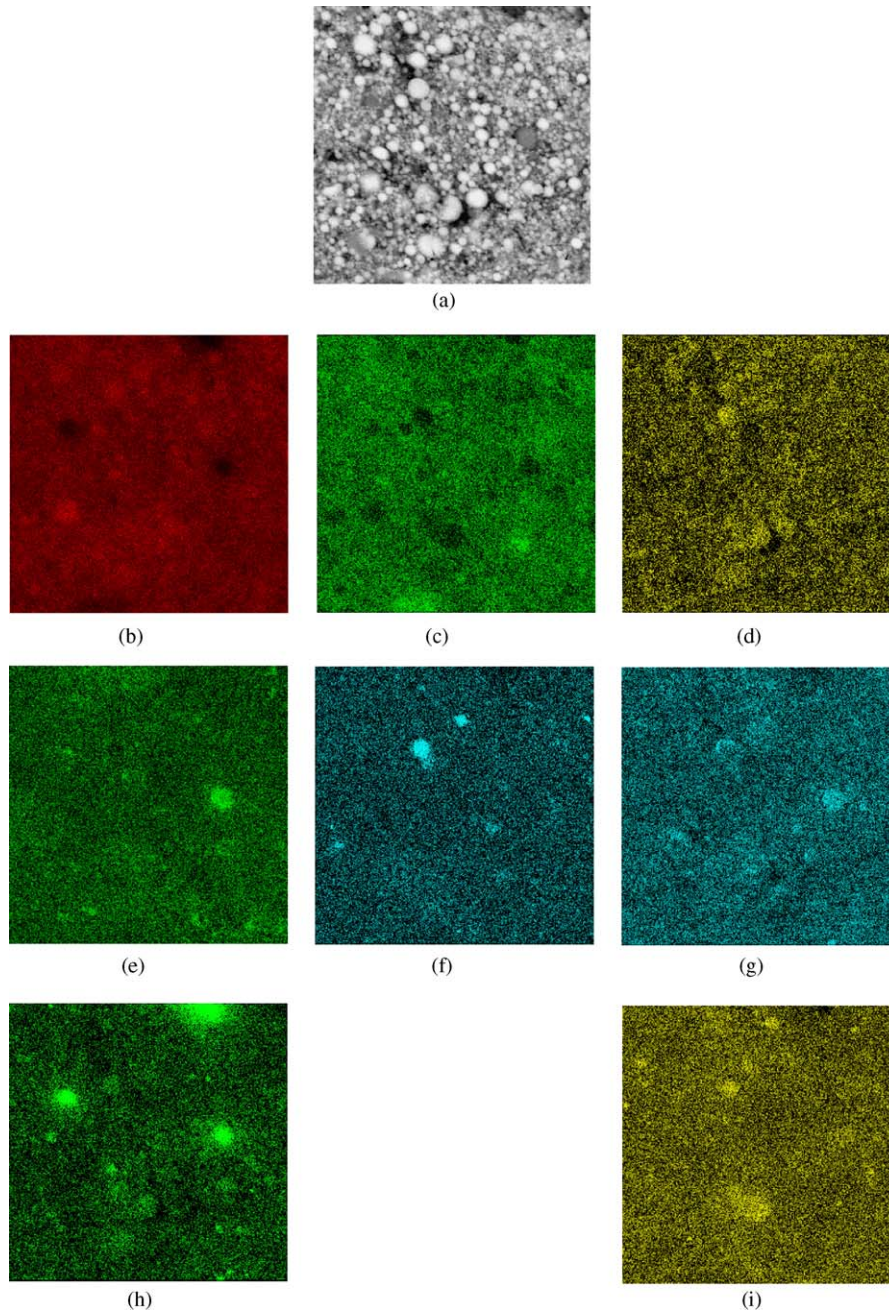


Fig. 9. SEM EDX mapping. (a) Secondary electron image of EAFD region, and distribution of (b) Fe, (c) Zn, (d) O, (e) Ca, (f) Cr, (g) Si, (h) Mg and (i) Mn.

presence of iron, zinc and oxygen elements is coincident, suggesting the existence of ZnFe_2O_4 phase. At the same time, it is also noted areas where zinc is not present, while iron is in a high amount. This fact suggests the presence of iron oxides, probably magnetite.

As it can be seen from Fig. 9, calcium is distributed in the EAFD in two regions, in one of them with iron and in the other one separated from this element. Calcium appears in high amount when iron is not present. In this area magnesium and silicon elements also appear. Probably, it is a phase rich in calcium, magnesium and silicon originated from fluxes added in

the steelmaking process. Besides, calcium appears distributed in lower concentration in regions where iron and oxygen are present, which can suggest the presence of the $\text{Ca}_{0,15}\text{Fe}_{2,85}\text{O}_4$ phase.

Fig. 9 shows that chromium is present in some regions with iron, which may suggest the presence of FeCr_2O_4 phase.

It was observed that magnesium appears forming phases with calcium and silicon elements. Magnesium is concentrated in regions where iron is not present. This fact confirms the result of the Mössbauer spectroscopy, which did not detect the MgFe_2O_4 phase in the EAFD.

4. Conclusions

- The mean particle diameter of EAFD was 1.88 μm . The EAFD has a heterogeneous distribution of particles, where 60% have size between 0.90 and 4.30 μm ;
- Fe and Zn are present in the EAFD with 49.96 and 9.24%, respectively;
- XRD technique detected in the EAFD the following phases: ZnFe_2O_4 , Fe_3O_4 , MgFe_2O_4 , FeCr_2O_4 , Mn_3O_4 , MgO , SiO_2 , $\text{Ca}_{0.15}\text{Fe}_{2.85}\text{O}_4$ and ZnO . However, except for SiO_2 and ZnO , the signals from all the phases exhibit overlapping. Because of such overlapping the presence of these phases cannot be unequivocally assured;
- The ferrous oxide phases detected by Mössbauer spectroscopy were: ZnFe_2O_4 , Fe_3O_4 , $\text{Ca}_{0.15}\text{Fe}_{2.85}\text{O}_4$ and FeCr_2O_4 ;
- MgFe_2O_4 phase was not observed in the Mössbauer spectrum. Such result is supported by ICP analysis and X-ray mapping analysis via SEM.

In conclusion, the characterization of a solid waste using many techniques increase the reliability in the results and also give more conditions to decide about the best feasible recycling method.

Acknowledgements

The authors would like to thank to CNPq for the financial support and GERDAU by handing EAFD sample for the study.

References

- [1] Associação Brasileira de Normas Técnicas (ABNT) NBR 10005. Lixiviação de resíduos-procedimentos. Rio de Janeiro, 1987.
- [2] Associação Brasileira de Normas Técnicas (ABNT) NBR 10004. Resíduos Sólidos, 09/1987.
- [3] F.A. Brehm, D.F. Graffitti, C.A.M. Moraes, A.C.F. Vilela, I.A. Mafaldo, Caracterização química, térmica e estrutural de pós de aciaria elétrica, in: XXXII Seminário de fusão, refino e solidificação dos metais, Salvador, 2001, pp. 67–75.
- [4] G.G. Néstor, G.E.V. Borja, The situation of EAF dust in Europe and the upgrading of the Waelz process. In: Global Symposium on Recycling, Waste Treatment and Clean Technology, Rewas, 99, vol. 2, pp. 1511–1520.
- [5] N. Leclerc, E. Meux, J.M. Lecuire, Hydrometallurgical extraction of zinc from zinc ferrites, Hydrometallurgy (2003) 175–183.
- [6] C. Takano, M.C. Mantovani, F.L. Cavallante, M.B. Mourão, Electric arc furnace dust characterization and recycling by self reducing pellets, in: First Japan–Brazil Symposium on dust processing-energy-environment in metallurgical industries, São Paulo, 1999.
- [7] F.A. Brehm, D.F. Graffitti, C.A.M. Moraes, A.C.F. Vilela, Desenvolvimento de um método para digestão de pós de aciaria elétrica com vistas à caracterização química do resíduo, in: Anais do Congresso em Ciência de Materiais do Mercosul, Sulmat, Joinville, SC, 2002, pp. 448–457.
- [8] G.J. Long, T.E. Cranshaw, G. Longworth, Mössbauer Eff. Data J. 6 (1983) 42–45.
- [9] M.C. Mantovani, C. Takano, F.L. Cavallante, Caracterização de três tipos de poeiras geradas em fornos elétricos a arco, in: 53 Congresso Anual da ABM 53, 1998, pp. 1329–1343.
- [10] D.K. Xia, C.A. Pickles, Microwave caustic leaching of electric arc furnace dust, Miner. Eng. 13 (2000) 79–94.
- [11] N. Menad, J.N. Ayala, F.G. Carcedo, E.R. Ayúcar, A. Hernández, Study of the presence of fluorine in the recycled fractions during carbothermal treatment of EAF dust, Waste Manage. (2003) 483–491.
- [12] M. Pelino, A. Karamanov, P. Piscicella, S. Crisucci, D. Zonetti, Vitrification of electric arc furnace dusts, Waste Manage. 22 (2002) 945–949.
- [13] Q. Yang, B. Gustafsson, Studies on dust recycling in the electric arc furnace at Uddeholm Tooling AB, Scand. J. Metall. (2003) 147–156.
- [14] A. Masud, A. Latif, Fundamentals of zinc recovery from metallurgical wastes in the enviroplas process, Miner. Eng. (2002) 945–952.
- [15] J.C. Huber, F. Patisson, P. Rocabois, J.P. Birat, D. Ablitzer, Some means to reduce emissions and improve the recovery of electric arc furnace dust by controlling the formation mechanisms. In: Global Symposium on Recycling, Waste Treatment and Clean Technology, Rewas'99, vol. 2, pp.1483–1491.
- [16] R.L. Nyrenda, The processing of steelmaking flue-dust: a review, Miner. Eng. Vol.4 (1991) 1003–1025.
- [17] N.C. Heck, M.I. Costa, J.V.V. Weber, Anais do 55º Congresso Annual da ABM, Rio de Janeiro, julho, 2000, pp. 2667–2675.
- [18] G.F. Goya, S.J. Stewart, R.C. Mercader, Mössbauer study of Fe–Zn–O phases, Solid State Commun. 96 (7) (1995) 485–490.
- [19] C.R. Bluncson, G.K. Thompson, B.J. Evans, ^{57}Fe Mössbauer investigations of manganese-containing spinels, Hyperfine Interact. 90 (1994) 353–358.
- [20] M.T.X. Silva, Aplicação do efeito Mössbauer à análise de amostras de basalto, Porto Alegre, 1977. Dissertação (Mestrado em Física) – Instituto de Física, Universidade Federal do Rio Grande do Sul, 1977.
- [21] S.M. Dubiel, J. Cieslak, J. Orewczyk, S. Jasienska, Mössbauer effect study of calciomagnetites, Acta Phys. Pol., A 93 (No. 3) (1998) 547–561.
- [22] C.M.O. Barcellos, Propriedades magnéticas e estruturais de goetitas dopadas com gálio. Porto Alegre, 2001. Dissertação (Mestrado em Física) – Instituto de Física, Universidade Federal do Rio Grande do Sul, 2001.
- [23] J.G.M.S. Machado, Estudo de caracterização e avaliação da influência do tempo na redução carbotérmica do pó de aciaria elétrica, Porto Alegre, 2004. Dissertação (Mestrado em Engenharia) – Escola de Engenharia, Universidade Federal do Rio Grande do Sul, 2004.
- [24] T. Sofilic, A.R. Mioc, S.C. Stefanovic, V.N. Radovic, M. Jenko, Characterization of steel mill electric-arc furnace dust, J. Hazard. Mater. (2004) 59–70.
- [25] M.C. Mantovani, C. Takano, P.M. Büchler, Electric arc furnace dust-coal composite pellet: effects of pellet size, dust composition, and additives on swelling and zinc removal, Ironmaking Steelmaking 29 (2002) 257–265.
- [26] M. Cruells, A. Roca, C. Núñez, Electric arc furnace flue dusts: characterization and leaching with sulphuric acid, Hydrometallurgy 31 (1992) 213–231.